



Achieving high-performance for catalytic epoxidation of styrene with uniform magnetically separable CoFe_2O_4 nanoparticles



Jiangyong Liu^{a,*}, Ru Meng^a, Jinxing Li^a, Panming Jian^a, Lixia Wang^a, Ruiqi Jian^b

^a School of Chemistry and Chemical Engineering, Yangzhou University, Yangzhou, Jiangsu 225002, China

^b School of Medicine, Stanford University, Stanford, CA 94304, USA

ARTICLE INFO

Keywords:

CoFe_2O_4
Nanoparticles
Styrene
Epoxidation
Bimetallic catalyst

ABSTRACT

Developing catalysts with unique compositional and structural characteristics, high cost-efficiency, and preferable catalytic performance are still an ongoing task for the selective oxidation of alkenes. Herein, we report the facile construction of uniform magnetically separable CoFe_2O_4 nanoparticles, which can function as an efficient and robust catalyst for the selective epoxidation of styrene with tert-butyl hydroperoxide as the oxidant. This bimetallic catalyst significantly outperformed its monometallic counterparts with respect to Co_3O_4 flakes and Fe_2O_3 rods both in terms of total activity and epoxide production. In the presence of CoFe_2O_4 nanoparticles as the catalyst, the yield of styrene oxide (SO) can achieve 79.7% with a total styrene conversion of 96.4% and a selectivity of 82.7% to SO under the optimal reaction condition. In addition, the activation energy was measured, and a plausible reaction mechanism was proposed. The outstanding catalytic performance of the CoFe_2O_4 catalyst can be ascribed to the synergistic effects regarding the abundant surface metal redox couples induced by the bimetallic nature and the mesoporous structure with high surface area.

1. Introduction

In recent years, bimetallic catalysts have attracted tremendous research interests both in academic and industrial circles since they usually exhibit new properties and capabilities when compared with those of their pure constituent metals (monometallic catalysts) due to the synergistic intermetallic interactions [1–10]. Such synergistic effects mainly originate from the ligand effect regarding the direct electron interactions between single metals and the strain effect with respect to the electronic structure change by the lattice strain change, which are beneficial for the enhancement of catalytic performances [11–13]. For example, Wang et al. [14] found that a $\text{Ni}_{0.67}\text{Co}_{0.33}(\text{OH})_2$ nanosheet array *in situ* grown on carbon cloth (CC) forming a $\text{Ni}_{0.67}\text{Co}_{0.33}(\text{OH})_2/\text{CC}$ anode presents a superior performance over those of $\text{Ni}(\text{OH})_2/\text{CC}$ or $\text{Co}(\text{OH})_2/\text{CC}$ in the urea oxidation reaction, suggesting that a synergistic effect of Ni and Co in boosting the catalytic activity. This synergistic effect was considered to be derived from the better electrical conductivity of the bimetallic catalyst, and the lattice distortion and subtle atomic rearrangement due to the mismatch in the degree of Jahn–Teller distortion that can offer more active sites in the reaction. Feng et al. [15] developed Au–Ag bimetallic catalysts deposited on titanium silicate-1 with blocked pores, and the results indicated that the synergy between Au and Ag reduced the Au

nanoparticle size and enhanced the oxygen adsorption and electron transfer ability from Au to oxygen, resulting in much better catalytic performance for propene epoxidation than those of the monometallic Au and Ag catalysts. Chen et al. [16] prepared NiCo_2O_4 nanoframes with a nanosheet surface presented much higher catalytic activity and stability for the oxygen evolution reaction than the Co_3O_4 and NiO nanoframes. The high surface area and the synergistic effect of Ni and Co were identified as the major contributors to the superior catalytic performance of the NiCo_2O_4 nanoframes. Luo et al. [17] prepared a series of Cu–Mn composite oxides, displaying a higher catalytic activity than the single metal oxides. The results showed that the active component for the carbonylation reaction of glycerol with urea was the $\text{Cu}_{1.4}\text{Mn}_{1.6}\text{O}_4$ crystal phase which can provide Mn^{4+} and lattice oxygen (O^{2-}), and the $\text{Mn}^{4+}–\text{O}^{2-}$ Lewis acid–base pair can contribute to the production of glycerol carbonate.

SO, as an industrially important chemical, is widely used in the synthesis of plasticizer, epoxy resins and perfumes, and is also a key organic intermediate for the manufacture of pharmaceuticals and fine chemicals [18–20]. SO is traditionally produced by the chlorohydrin process or the oxidation with peracids as the oxidizing agent [21,22]. Unfortunately, these processes are environmentally unfriendly, which are associated with the generation of enormous amount of toxic and corrosive chemical waste [22]. Recently, the selective oxidation of

* Corresponding author.

E-mail address: liujy@yzu.edu.cn (J. Liu).

styrene by green oxidants such as molecular oxygen, hydrogen peroxide and tert-butyl hydroperoxide has aroused great attention both academically and industrially [23–27]. Although both the homogeneous catalysts and heterogeneous catalysts have been employed for the oxidation of styrene, the former ones have received less attention due to the complicated recovery and recycling problems. Therefore, on account of the inherent advantages of heterogeneous catalysts over homogeneous ones, various solid catalysts have been developed, among which Co and Fe-based catalysts have attracted extensive attention [18,28–36]. Among them, some catalysts exhibited high catalytic activity or good SO selectivity, but the possibility to achieve attractive activity and selectivity at the same time is very limited. On the other hand, the further application of some of these catalysts can be impeded by the tedious, uneconomical and/or complex preparation processes. These challenges promote us to explore a high-performance catalyst for the selective oxidation of styrene with a facile preparation procedure.

In this work, we obtained uniform CoFe_2O_4 nanoparticles prepared by a facile one-pot hydrothermal process. The bimetallic CoFe_2O_4 catalyst can function as a very efficient catalyst for the selective oxidation of styrene, exhibiting a much better performance than the mono-metallic Co_3O_4 and Fe_2O_3 catalyst. In addition, various reaction parameters, including reaction temperature, catalyst amount, styrene/TBHP molar ratio, solvent type and addition of urea on the catalytic performances were fully investigated to screen the optimum reaction and find a way for the product regulation.

Under the optimum reaction condition, a high SO yield of 79.7% with a styrene conversion of 96.4% and a high selectivity of 82.7% to SO were obtained. Furthermore, the kinetic analysis was conducted, and the reaction mechanism was proposed for a better understanding of the reaction process.

2. Experimental

2.1. Catalyst preparation

The CoFe_2O_4 nanoparticles were prepared by a facile one-pot hydrothermal method. In a typical synthesis, 2.5 mmol of $\text{Co}(\text{NO}_3)_2 \cdot 6\text{H}_2\text{O}$ and 5.0 mmol of $\text{Fe}(\text{NO}_3)_3 \cdot 9\text{H}_2\text{O}$ were dissolved in 40 ml of deionized (DI) water. Then 0.75 g of polyvinylpyrrolidone (PVP) K30 was added to the above solution under magnetic stirring for 30 min. Afterwards, the pH of the solution was adjusted to 12 by dropwise addition of 2 M KOH and kept on stirring for 1 h. And then, the mixture was transferred into a Teflon-lined stainless-steel autoclave for hydrothermal treatment at 180 °C for 9 h before cooling down to room temperature naturally. The resulting black precipitate was collected by filtration and washed thoroughly with DI water and ethanol repeatedly. Finally, the product was dried at 80 °C for 12 h and calcined at 500 °C for 2 h. For a better comparison, pure Co_3O_4 and Fe_2O_3 were prepared as well under similar synthesis conditions with either $\text{Co}(\text{NO}_3)_2 \cdot 6\text{H}_2\text{O}$ or $\text{Fe}(\text{NO}_3)_3 \cdot 9\text{H}_2\text{O}$ added in the reaction mixture.

2.2. Catalyst characterization

The X-ray powder diffraction (XRD) analysis was conducted on a D8 Advance diffractometer using $\text{Cu K}\alpha$ radiation in the 20 range of 10–80°. The metal composition in the CoFe_2O_4 sample was analyzed using inductively coupled plasma atomic emission spectroscopy (ICP-AES, Optima 8300, PerkinElmer, Waltham, USA). The Scanning electron microscopy (SEM) images were obtained on a Hitachi S-4800 field-emission scanning electron microscope at a voltage of 5 kV. The transmission electron microscopy (TEM) and high-resolution TEM (HRTEM) images were recorded using a JEM-2100 microscope equipped with an energy-diffusive X-ray spectroscopy (EDS) attachment. The X-ray photoelectron spectroscopy (XPS) data were obtained on a Thermo, Fisher Scientific ESCALAB 250Xi spectrometer. The Raman spectra were collected on a Renishaw inVia laser Raman

spectrometer. The N_2 adsorption–desorption measurements were carried out on a Quantachrome Autosorb-iQ3 sorption analyzer. The magnetic characterization was performed by vibrating sample magnetometer (VSM, ADE-EV7).

2.3. Catalytic test

The styrene oxidation reaction was carried out in a three-necked glass flask equipped with a reflux condenser. In a typical reaction, a certain amount of styrene, solvent and catalyst were added into the flask under stirring. After heating the reaction mixture to a desired temperature, a certain amount of tert-butyl hydroperoxide (TBHP, 65 wt.% in water) was added dropwise to the reaction mixture to trigger the reaction. Various experiments regarding the effects of reaction temperature, catalyst amount, styrene/TBHP molar ratio, solvent type and addition of urea on the catalytic performances were carried out. Each reaction was repeated at least twice to ensure the accuracy of data. For the recycling test, the used catalyst was magnetically separated, washed with ethanol, dried at 100 °C for 24 h, and applied in the next run. For the kinetic study, the reaction results at different reaction temperatures of 60, 70, 80 and 90 °C were further processed to get the apparent rate constant and apparent activation energy. After reaction, the suspension was magnetically separated and then analyzed by a gas chromatography using a flame ionization detector equipped with a KB-1 column. The carrier gas was N_2 , and toluene was selected as an internal standard. The selectivity of the products in the reaction system was calculated in terms of mol percentage, and the carbon balance was within 100 ± 4%. The styrene conversion, SO selectivity and SO yield were calculated by the following equations:

$$\text{Styrene conversion (\%)} = (\text{converted styrene in molar} / \text{initial styrene in molar}) \times 100\%.$$

$$\text{SO selectivity (\%)} = (\text{SO in the product in molar} / \text{converted styrene in molar}) \times 100\%.$$

$$\text{SO yield (\%)} = \text{conversion (\%)} \times \text{SO Selectivity (\%)} / 100$$

3. Results and discussion

3.1. Phase, texture and morphology

Fig. 1a shows the XRD patterns of the CoFe_2O_4 , Co_3O_4 and Fe_2O_3 samples. The characteristic diffraction peaks observed at 24.1°, 33.2°, 35.6°, 40.9°, 49.5°, 54.1°, 62.4° and 64.0° can be assigned to the (012), (104), (110), (113), (024), (116), (214) and (300) planes of the hexagonal $\alpha\text{-Fe}_2\text{O}_3$, respectively, which are consistent with the standard spectrum (JCPDS card No. 33-0664). The peaks at 19.0°, 31.3°, 36.8°, 44.8°, 55.7°, 59.4° and 65.2° can be identified for the (111), (220), (311), (400), (422), (511) and (440) planes of the spinel Co_3O_4 , respectively (JCPDS card No. 42-1467). And the characteristic peaks observed at 18.2°, 30.1°, 35.5°, 43.5°, 53.9°, 57.2° and 62.7° correspond to the (111), (220), (311), (400), (422), (511) and (440) planes of the spinel CoFe_2O_4 , respectively (JCPDS card No. 22-1086). The XRD pattern of the spinel CoFe_2O_4 is similar with that of the pure spinel Co_3O_4 , but with a left shift toward lower diffraction angles. This indicates that the incorporation of Fe can result in lattice deformation due to the different ion radius of Fe and Co since the lattice of Co_3O_4 can host many other metal cations with partial substitution of Co [37]. In addition, the Fe/Co molar ratio in the CoFe_2O_4 sample obtained by the ICP-AES analysis is 1.99, which is very close to the theoretical value. The estimated crystallite size of the CoFe_2O_4 is calculated to be 17.6 nm from the full-width at half-maximum (FWHM) of the peak (311) using the Scherrer equation. Fig. 1b shows the Raman spectrum of the CoFe_2O_4 nanoparticles. The distinguishable five peaks can be assigned to the single phase of CoFe_2O_4 with a O_h^7 symmetry ($\text{Fd}3m$ space group)

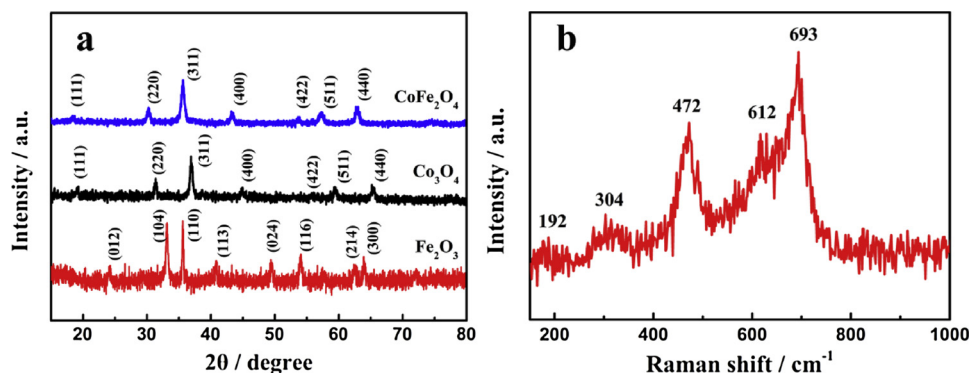


Fig. 1. XRD patterns of the samples (a) and Raman spectrum (b) of the CoFe_2O_4 .

[38]. The two peaks at 693 cm^{-1} ($\text{A}_{1g}(1)$) and 612 cm^{-1} ($\text{A}_{1g}(2)$) can be attributed to the symmetric stretching of the oxygen atoms with respect to metal ions in the tetrahedral void [39]. The other low frequency modes at 472 cm^{-1} (T_{2g}), 304 cm^{-1} (E_g) and 192 cm^{-1} (T_{2g}) correspond to the symmetric and antisymmetric stretching of the oxygen atoms with respect to metal ions in the octahedral void [40]. These results further demonstrate that the obtained composite sample is pure CoFe_2O_4 with a cubic inverse spinel structure.

Fig. 2(a–c) presents the representative SEM images of the Co_3O_4 , Fe_2O_3 and CoFe_2O_4 , respectively. Interestingly, the three samples exhibit quite different morphologies, suggesting the importance of metal species in the hydrothermal synthesis. The Co_3O_4 shows a two-dimensional polygonal flake structure, the Fe_2O_3 shows a one-dimensional rod shape, while the CoFe_2O_4 is composed of uniform three-dimensional nanoparticles. The TEM image of the CoFe_2O_4 in Fig. 2d further displays the homogeneous CoFe_2O_4 nanoparticles which have a narrow particle size distribution with the mean particle size measured to be 13.5 nm derived from the statistical TEM data analysis (Fig. 2d, inset). This value is slightly smaller than the one obtained from the XRD analysis (17.6 nm). The clear lattice fringes with interplane spacing of 0.485 , 0.297 and 0.253 nm can be attributed to the (111) , (220) and

(311) planes for the CoFe_2O_4 nanoparticles, respectively (Fig. 2e). The EDS elemental mapping in Fig. 2f shows that the Co, Fe and O elements are evenly distributed in the CoFe_2O_4 nanoparticles.

Fig. 3a shows the N_2 adsorption–desorption isotherms of the Fe_2O_3 , Co_3O_4 and CoFe_2O_4 . All the samples show a type IV isotherm, indicating their mesoporous structure. The surface area of the CoFe_2O_4 measured with the Brunauer–Emmett–Teller (BET) method [41] is $65.6\text{ m}^2\text{ g}^{-1}$, which is much higher than those for the Fe_2O_3 ($38.0\text{ m}^2\text{ g}^{-1}$) and Co_3O_4 ($34.9\text{ m}^2\text{ g}^{-1}$) prepared by similar hydrothermal methods. The mean pore size obtained by the Barrett–Joyner–Halenda (BJH) method [42] from the desorption branches of the isotherms (Fig. 3b) is 12.3 nm for the CoFe_2O_4 , which is also larger than those for the Fe_2O_3 (3.3 nm) and Co_3O_4 (3.0 nm). The high surface area and large pore size play important roles in the catalytic reaction since these merits can not only provide abundant catalytically active sites, but also facilitate the diffusion of reactants and products within the channels.

To further investigate the surface elemental composition and determine the chemical state of individual elements of the CoFe_2O_4 nanoparticles, the XPS analysis was carried out. As expected, the XPS survey shows the existence of the Co and Fe in the CoFe_2O_4 (Fig. 4a).

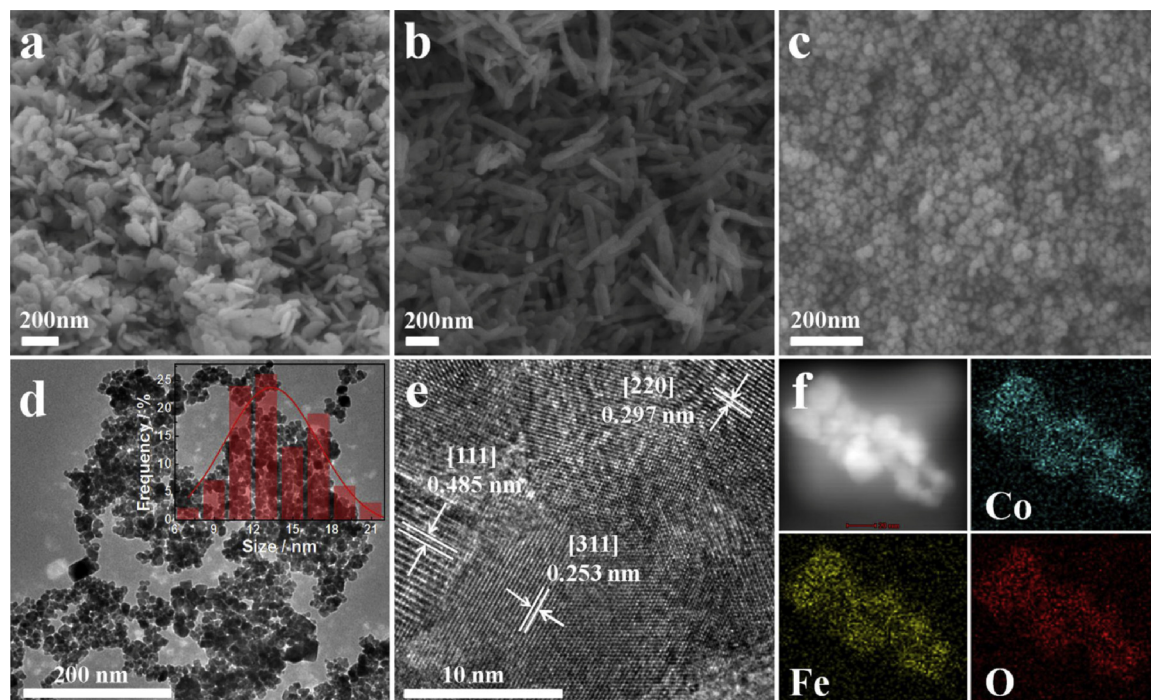


Fig. 2. SEM images of the Co_3O_4 (a), Fe_2O_3 (b) and CoFe_2O_4 (c); TEM image (d), HRTEM image (e) and EDS elemental mapping (f) of the CoFe_2O_4 nanoparticles. The inset in (d) shows the particle size distribution of the CoFe_2O_4 nanoparticles.

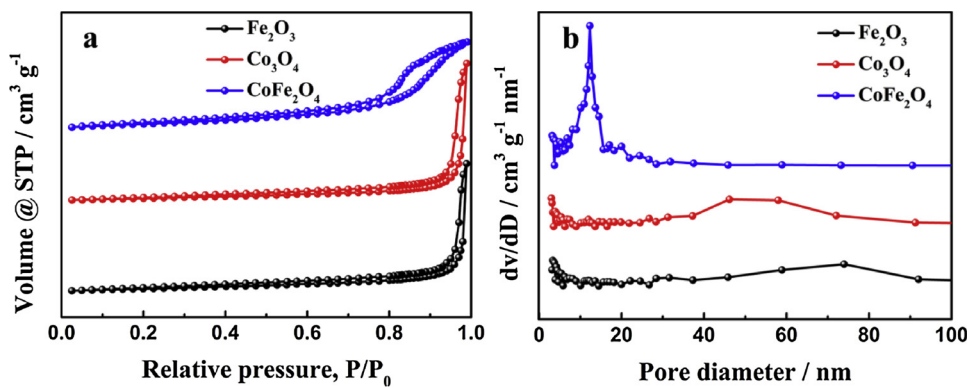


Fig. 3. Nitrogen adsorption–desorption isotherms (a) and the corresponding BJH pore size distributions (b) of the samples.

Fig. 4b shows the high-resolution XPS Co 2p spectrum, in which two main signals of $\text{Co} 2p_{3/2}$ and $\text{Co} 2p_{1/2}$ were observed at 779.8 eV and 795.3 eV, respectively. With a Gaussian fit, the Co 2p spectrum can be well fitted into two peaks at 782.2 and 796.5 eV corresponding to Co^{2+} , two peaks at 779.8 and 795.2 eV assigned to Co^{3+} , and the other two peaks attributed to shakeup satellites [43,44]. The high-resolution XPS Fe 2p spectrum depicted in Fig. 4c is consisted of two spin-orbit doublets attributable to $\text{Fe} 2p_{3/2}$ and $\text{Fe} 2p_{1/2}$. The fitted two peaks at 710.5 and 723.9 eV can be assigned to the contributions from Fe^{3+} in the octahedral sites, while the two peaks at 712.6 and 726.3 eV can be due to the contributions from Fe^{3+} in the tetrahedral sites [45]. In addition, the presence of the shake-up satellite between $\text{Fe} 2p_{3/2}$ and $\text{Fe} 2p_{1/2}$ can be an evidence for the presence of Fe^{2+} [46,47]. This indicates that Fe in the CoFe_2O_4 exists mainly in Fe^{3+} with little Fe^{2+} . The O 1s spectrum (Fig. 4d) can be fitted into two peaks, with the one at 530.0 eV assigned to surface lattice oxygen in the metal–oxygen bond and the other one at 531.5 eV corresponding to the adsorbed O– or O_2^{2-} species and hydroxyl groups which are associated with the intrinsic oxygen vacancies on the surface [48]. These redox couples of Co^{2+} /

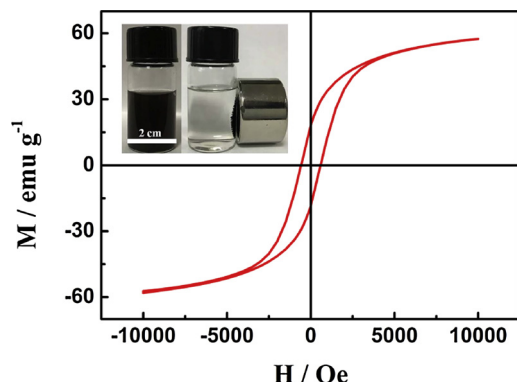


Fig. 5. Room-temperature M – H hysteresis loop of the CoFe_2O_4 nanoparticles. The inset shows the images of CoFe_2O_4 suspension without (left) and with (right) a magnetic field.

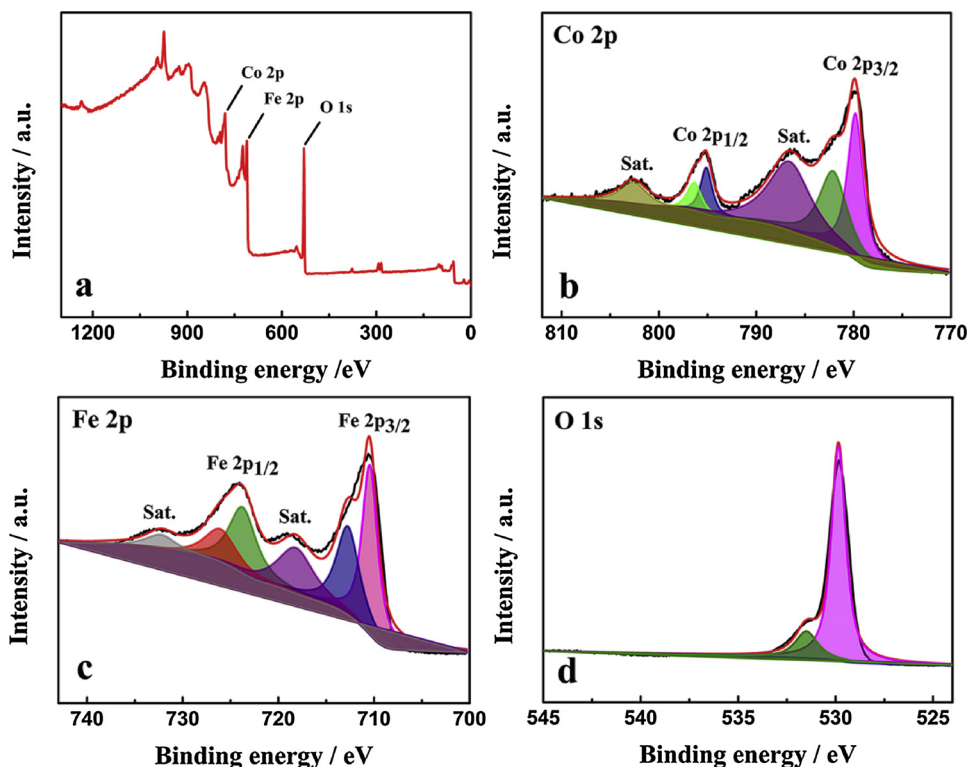


Fig. 4. XPS survey (a), high-resolution Co 2p spectrum (b), Fe 2p spectrum (c) and O 1s spectrum (d) of the CoFe_2O_4 .

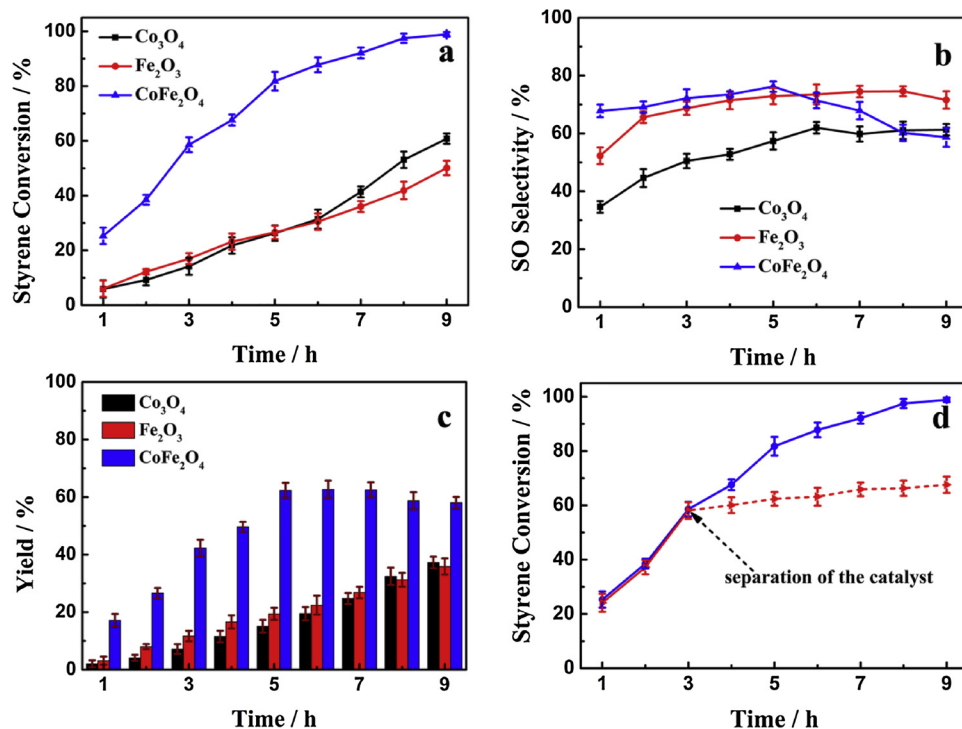


Fig. 6. (a–c) Evaluation of the catalytic performances of the CoFe_2O_4 , Fe_2O_3 and Co_3O_4 catalyst. Reaction condition: 15 mmol styrene, 0.1 g catalyst, 16 ml acetonitrile, 45 mmol TBHP, 80 °C, 9 h. (d) Evidence of heterogeneous catalysis of CoFe_2O_4 in the oxidation of styrene.

Co^{3+} and $\text{Fe}^{2+}/\text{Fe}^{3+}$ and surface oxygen species in the CoFe_2O_4 catalyst can be beneficial for the oxidation reactions.

Fig. 5 shows the M - H hysteresis loop of the CoFe_2O_4 catalyst at room-temperature, indicating its ferromagnetic characteristic. As observed, the saturation magnetization (M_s) value is 57.5 emu g^{-1} , which is smaller than the bulk value (74.08 emu g^{-1}) [49]. This can also suggest the small particle size of the CoFe_2O_4 nanoparticles, as verified by the XRD and TEM analysis [50]. The coercivity of the CoFe_2O_4 is measured to be 596 Oe, suggesting that it can be easily separated from the reaction mixture through inducing an external magnetic field (Fig. 5, inset).

3.2. Catalytic performance

The CoFe_2O_4 nanoparticles were tested in the oxidation of styrene with TBHP as the oxidant. For comparison, the Co_3O_4 flakes and Fe_2O_3 rods were tested as well under the same reaction conditions. SO and benzaldehyde were found to be the main products with little benzoic acid, phenylacetaldehyde and 1-phenyl-1, 2-ethanediol as the by-products. Fig. 6a shows the plotting of styrene conversion *versus* reaction time. For all the three catalysts, the styrene conversion increases steadily with the reaction time. Noticeably, the CoFe_2O_4 presents a highest initial activity, and the conversion of styrene quickly reaches 58.6% in the first 3 h and then increases continuously to 100% within a reaction duration of 9 h despite the sluggish increase after 7 h. This conversion value of 100% is much higher than those for the Co_3O_4 (60.8%) and Fe_2O_3 (50.1%). However, the SO selectivity *versus* reaction time (Fig. 6b) doesn't show the same trend as that of the styrene conversion. The SO selectivity first increases slowly with the reaction time and then decreases after passing through a maximum for all the three catalysts. The decrease of the SO selectivity is mainly due to the over-oxidation of SO and the hydrolysis of SO into 1-phenyl-1, 2-ethanediol [31,51]. And thus the yield of SO exhibits a volcano-type relationship with respect to the reaction time (Fig. 6c). The highest yield of SO for the CoFe_2O_4 obtained at 5 h is 62.3%, with a styrene conversion of 81.8% and SO selectivity of 76.2%. This yield value of 62.3% is 3.13 times than that

for the Co_3O_4 (15.1%) and 2.21 times than that for the Fe_2O_3 (19.4%), indicating a very pronounced synergistic effect between Co and Fe in the bimetallic CoFe_2O_4 catalyst. In order to figure out if the leaching of metal ions from the catalyst took place during the reaction, the CoFe_2O_4 catalyst was magnetically separated from the reaction mixture after 3 h of reaction, and the reaction was continued without catalyst for another 6 h. The results indicated that no significant enhancement in the styrene conversion was observed with additional 6 h of reaction. In addition, ICP analysis of the solution after the reaction did not show the presence of cobalt and iron. These results suggest that no metal leaching occurred within the reaction duration, and the selective oxidation of styrene in the presence of the CoFe_2O_4 catalyst is driven by heterogeneous catalysis. What's more, with an aim to screen the best reaction condition and gain insights into the reaction mechanism, the CoFe_2O_4 catalyst was tested under various reaction conditions for the selective oxidation of styrene into SO.

3.2.1. Effect of the reaction temperature

To investigate the effect of reaction temperature on the catalytic performance, the reaction was performed at temperatures ranging from 60 to 90 °C, and the results are summarized in Fig. 7a. As expected, the styrene conversion increases with increase in the reaction temperature, while the SO selectivity *versus* reaction temperature shows an opposite trend. The high temperature can be beneficial for the reaction rate, but can also induce more side reactions with the generation of more unwanted by-products [18,51], and thus an optimal reaction temperature should exist. Taking both the catalytic activity and selectivity into consideration, 80 °C was selected as the reaction temperature for further investigations of the other important reaction parameters.

3.2.2. Effect of catalyst amount

To study the effect of catalyst amount on the styrene conversion and SO selectivity, we changed the amount of catalyst from 0.05 to 0.2 g while keeping the other reaction parameters constant. With an increase in catalyst amount from 0.05 to 0.15 g, the styrene conversion can be remarkably increased from 45.3% to 90.4% since more necessary

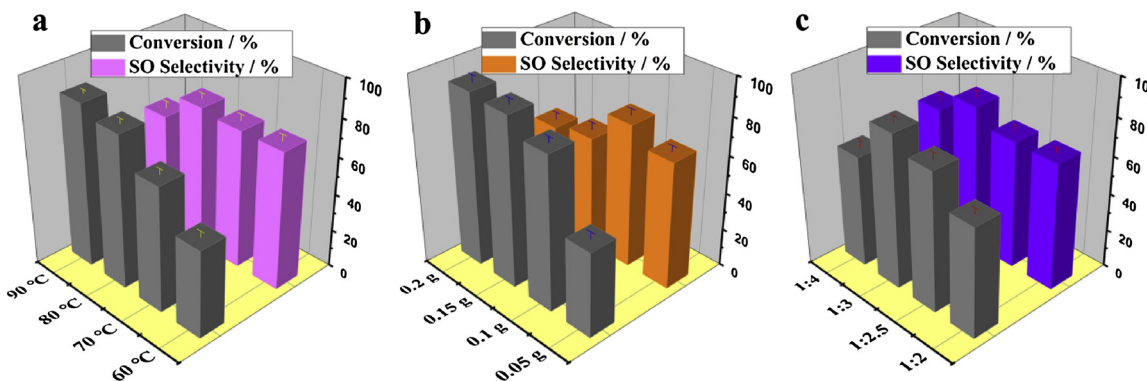


Fig. 7. The effects of reaction temperature (a), catalyst amount (b) and molar ratio of styrene/TBHP (c) on the catalytic performances of the CoFe_2O_4 catalyst. Reaction condition: (a) 15 mmol styrene, 0.1 g CoFe_2O_4 , 16 ml acetonitrile, 45 mmol TBHP, 5 h; (b) 15 mmol styrene, 16 ml acetonitrile, 45 mmol TBHP, 80 °C, 5 h; (c) 15 mmol styrene, 0.1 g CoFe_2O_4 , 16 ml acetonitrile, 80 °C, 5 h.

catalytic sites for the reaction can be afforded with more catalyst involved (Fig. 7b). And the conversion value further shows a slight increase to 92.1% when the catalyst amount was further increased to 0.2 g. However, this single rising tendency is not true for the SO selectivity. The plotting of SO selectivity with respect to the catalyst amount shows a volcano-shaped curve, with the highest value obtained at 0.1 g. In addition, it is widely accepted that using a large amount of catalyst is not economically viable for a practical application. Therefore, 0.1 g of catalyst was chosen as an optimum parameter for further research.

3.2.3. Effect of molar ratio of styrene/TBHP

The effect of molar ratio of styrene to TBHP on the catalytic performance was examined by keeping the amount of styrene constant while changing the amount of TBHP. As shown in Fig. 7c, the styrene conversion increased from 58.4% to 81.8% when the styrene/TBHP molar ratio was decreased from 1:2 to 1:3. However, it does not mean that the more oxidant added, the better the catalytic activity since the styrene conversion decreased to 59.4% when the styrene/TBHP molar ratio was further decreased to 1:4. In addition, excess TBHP can also be disadvantageous for the SO selectivity although the styrene/TBHP molar ratio has less effect on the product selectivity as compared with that on the catalytic activity. When superfluous TBHP is added as the oxidant, a large occupation of the active sites by TBHP will take place, and thus little accessible sites are left for styrene, and also may lead to the further oxidation of SO into undesired byproducts. Therefore, the ratio of 1:3 was selected as the optimal value in this study.

3.2.4. Effect of the solvents

The choice of solvents is very important in heterogeneous catalytic reactions since solvents can interact with or modify the catalyst surface and influence the accessibility of active sites [23]. The effect of different solvents on the oxidation of styrene was studied by using various types of solvents as shown in Table 1. Acetonitrile was found to give the

highest styrene conversion and SO selectivity. Other solvents, i.e., dimethylacetamide, ethanol, dimethylformamide and acetone, show low catalytic activity (< 42%) and SO selectivity (< 60%). In the presence of ethanol as the solvent, benzaldehyde turns out to be the main product. Previous study has shown that acetonitrile as a polar solvent with a slight basicity can reduce the possibility of the open-ring reaction of SO to benzaldehyde, resulting in an enhancement of the SO selectivity [52]. Therefore, acetonitrile is considered to be a favorable solvent for the epoxidation of styrene.

3.2.5. Effect of the addition of urea in the reaction system

The finding that the basicity of acetonitrile may promote the selectivity of SO inspired us to investigate the effect of basicity of the reaction system on the catalytic performance. To achieve this, various amounts of urea were added in the reaction mixture since the slow hydrolysis of urea can gradually produce alkaline media and will not introduce alkali metal impurities. As observed, the addition of urea has little effect on the catalytic activity (Fig. 8a), but can effectively enhance the generation of SO and slow down the decreasing rate of SO selectivity within the reaction duration of 9 h (Fig. 8b). The addition of urea can protect the formed SO by suppressing the acid-catalyzed side reactions such as the isomerization, open-ring and hydrolysis reactions of SO since urea can act as a dehydrating agent as well as buffer for the reaction system [21,52–54]. When 0.4 g of urea was initially added in the reaction mixture, the yield of SO can reach 79.7% (Fig. 8c) with a styrene conversion of 96.4% and SO selectivity of 82.7% at a reaction duration of 8 h. Therefore, with an aim to improve the SO selectivity, 0.4 g of urea should be added when conducting experiments for the selective oxidation of styrene.

So far, we have systematically investigated the effects of reaction temperature, catalyst amount, styrene/TBHP molar ratio, solvent type and addition of urea on the catalytic performances of the styrene oxidation reaction. The optimal reaction condition can be illustrated as follows: reaction temperature of 80 °C, reaction time of 8 h, 0.1 g of CoFe_2O_4 catalyst, styrene/TBHP molar ratio of 1:3, acetonitrile as the solvent and addition of 0.4 g urea. Under this reaction condition, the yield of SO can achieve 79.7% with a total styrene conversion of 96.4% and a selectivity of 82.7% to SO. This yield value is better than those of the previously reported catalysts such as mesoporous Co_3O_4 (8.3%) [18], $\text{Ce}_{0.95}\text{Zr}_{0.05}\text{O}_2$ (22.0%) [55], CoO (34.6%) [30], $\text{CoO}_x/\text{TiO}_2/\text{SBA-15}$ (54.3%) [29] and $\alpha\text{-Fe}_2\text{O}_3$ (55.8%) [35], and comparable to or even better than those of precious metal catalysts such as $\text{Au}/\text{CaO}(\text{HDP})$ (32.9%) [56], $\text{Au}/\text{Fe}_3\text{O}_4$ (54.9%) [57] and $\text{Ag}/\text{KOH-}\gamma\text{-Fe}_2\text{O}_3$ (80.3%) [58].

3.3. Recycling performance of the catalyst

Catalyst recyclability is a big challenge in heterogeneous catalysis

Table 1
The effect of different solvents on the catalytic performances ^a.

Entry	Solvent	Conversion (%)	Selectivity (%)		
			SO	Benzaldehyde	Others
1	Acetonitrile	81.8	76.2	22.3	1.5
2	Dimethylacetamide	41.8	55.4	40.6	4.0
3	Ethanol	38.4	42.2	54.3	3.5
4	Dimethylformamide	30.0	57.8	38.0	4.2
5	Acetone	29.0	59.0	38.7	2.3

^a Reaction condition: 15 mmol styrene, 0.1 g CoFe_2O_4 , 16 ml solvent, 45 mmol TBHP, 80 °C, 5 h.

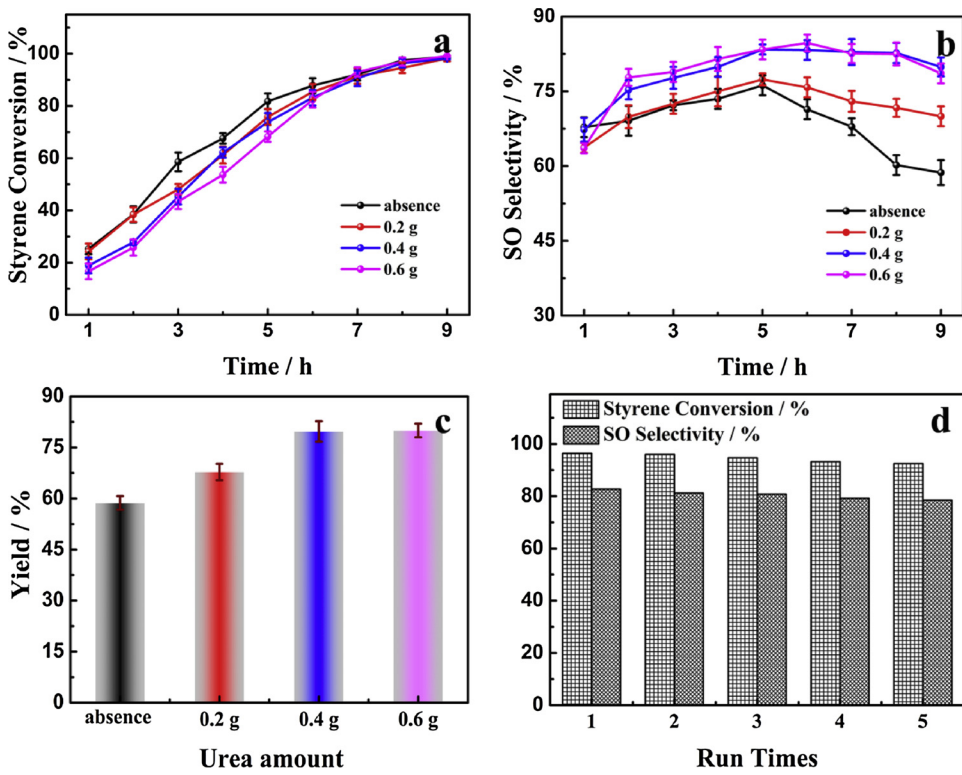


Fig. 8. (a–c) Evaluation of the effect of addition of urea on the catalytic performance of the CoFe_2O_4 catalyst. Reaction condition: 15 mmol styrene, 0.1 g CoFe_2O_4 , 16 ml acetonitrile, 45 mmol TBHP, 80 °C, 9 h. (d) Recycling performance of the CoFe_2O_4 catalyst. Reaction condition: 15 mmol styrene, 0.1 g CoFe_2O_4 , 16 ml acetonitrile, 45 mmol TBHP, 0.4 g urea, 80 °C, 8 h.

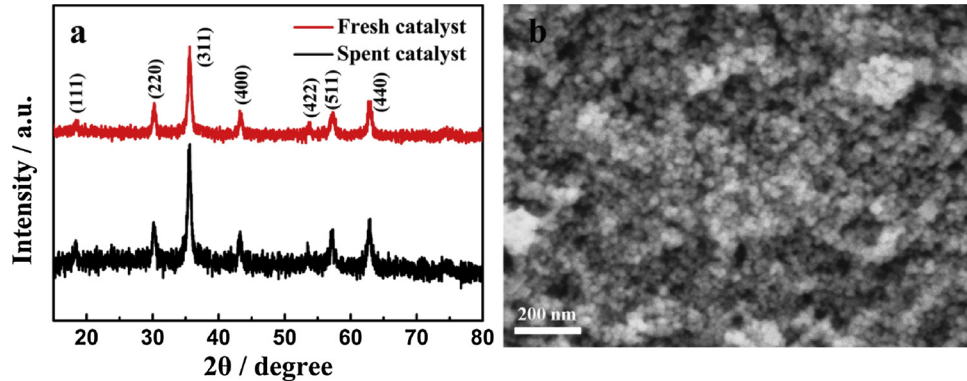


Fig. 9. XRD pattern (a) and SEM image (b) of the spent CoFe_2O_4 catalyst.

and an important parameter that should be required for the assessment of a catalyst [59]. The CoFe_2O_4 nanoparticles developed herein can be efficiently separated from the reaction mixture by an external magnetic field (Fig. 5, inset). The magnetic separation makes the recovery of the CoFe_2O_4 catalyst much easier as compared with the traditional methods such as filtration and centrifugation. Both the catalytic activity and SO selectivity in Fig. 8d show slight decrease after five consecutive runs with the same batch of catalyst, suggesting a good reusability of the CoFe_2O_4 catalyst. In addition, ICP analysis of the reaction mixture after the separation of catalyst did not show the presence of metal species. Furthermore, the XRD pattern (Fig. 9a) and SEM image (Fig. 9b) of the spent catalyst have no obvious changes with those of the fresh catalyst. All these results demonstrate that the uniform CoFe_2O_4 nanoparticles are efficient and stable for the styrene oxidation reaction.

3.4. Kinetics and mechanism

Kinetics studies of the CoFe_2O_4 catalyst at various temperatures show that pseudo-first-order kinetics can be applied for the evaluation of the catalytic rate as the data obtained experimentally can fit well

with the calculated ones (Fig. 10a). Hence, the kinetic equation for the reaction can be expressed as

$$-\ln\left(\frac{C}{C_0}\right) = kt \quad (1)$$

where k is the apparent rate constant; t is the reaction time; C_0 and C are the initial concentration of styrene and the concentration of styrene at time t , respectively. From the slopes of these fitted lines, the k values for the reactions performed at 60, 70, 80 and 90 °C can be calculated to be 0.1237, 0.2229, 0.3465, 0.4354 h^{-1} , respectively.

Further, the apparent activation energy (E_a) can be calculated by the Arrhenius equation

$$\ln k = \ln A - \frac{E_a}{RT} \quad (2)$$

where ($R = 8.314 \text{ J/(K·mol)}$) is the molar gas constant, A is the pre-exponential factor and T is the reaction temperature. From the slope of the fitted line regarding $\ln k$ versus $1000/T$ (Fig. 10b), the E_a value for the styrene oxidation reaction with the CoFe_2O_4 catalyst can be calculated to be 42.4 kJ/mol , which is comparable with the previously

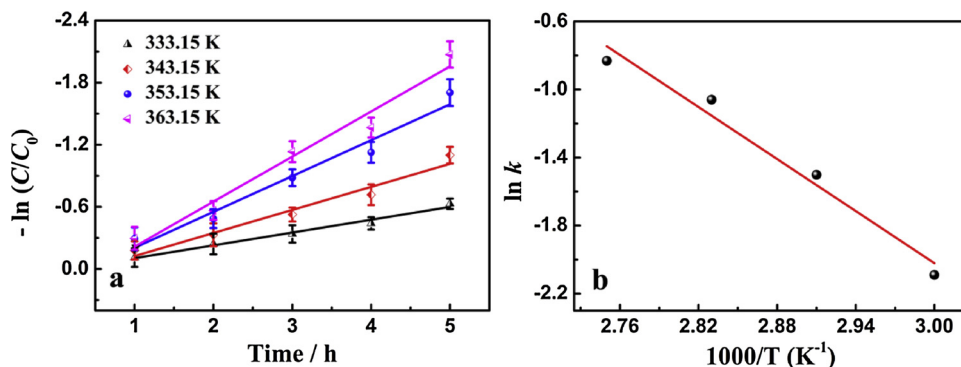


Fig. 10. $\ln(C/C_0)$ versus reaction time (a) and Arrhenius plot (b) of the styrene oxidation reactions performed at different temperatures.

reported values [60,61].

The proposed mechanism for the styrene oxidation reaction with the CoFe_2O_4 nanoparticles as the catalyst, depending on the previous studies [21,60,62] and the observed data in this work, are presented in Scheme S1. Firstly, the M (II) (M = Co, Fe) cations coordinate with the activated TBHP molecules by continuous interactions, giving a M (III) OO^\bullet superoxo type complex. Then, the complex will attack the double bond of styrene and undergo migratory insertion to form the peroxy metalallocycle, followed by the generation of four membered cyclic intermediate and the simultaneous release of M (II) species. The cyclic peroxy intermediate then further interacts with another styrene to form styrene oxide as the aimed product or decompose into benzaldehyde. The enhanced basicity of the reaction system by addition of urea may stabilize the cyclic peroxy intermediate. Therefore, the pathway with respect to the unwanted decomposition into benzaldehyde can be effectively suppressed, and thus a high selectivity of SO can be achieved.

The fact that the bimetallic CoFe_2O_4 nanoparticles significantly surpass the monometallic counterparts, i. e. Co_3O_4 flakes and Fe_2O_3 rods can be attributed to several possible reasons. Firstly, as indicated in Scheme S1, the synergistic interactions between surface $\text{Co}^{2+}/\text{Co}^{3+}$ redox pairs and $\text{Fe}^{2+}/\text{Fe}^{3+}$ redox pairs can accelerate the kinetics of the surface redox reactions, which is beneficial for the oxidation reactions [62–65]. Secondly, the large surface area of the CoFe_2O_4 nanoparticles can enhance the adsorption of reactants on the catalyst surface and benefit the exposure of more active sites for the catalytic reaction, and thus allow more efficient contact between the reactants and active sites. This can be verified from the reaction results of the CoFe_2O_4 catalysts calcined at higher temperatures of 600, 700 and 800 °C. The XRD patterns (Fig. S1) and SEM images (Fig. S2) show that the CoFe_2O_4 catalysts obtained at higher temperatures show higher crystallinity and larger particle size. In addition, as shown in Table S1, a higher calcination temperature induces a lower BET surface area. As expected, the yield of SO exhibits obviously positive correlations with the BET surface area, which manifests the importance catalyst surface area on the catalytic performance of the styrene oxidation reaction. In addition, the large pore size of the CoFe_2O_4 catalyst can decrease the pore diffusion resistance of the reactants, further promoting the accessibility of reactants to the catalytic sites.

4. Conclusions

In conclusion, uniform CoFe_2O_4 nanoparticles have been facilely developed and employed as an attractive catalyst for the selective oxidation of styrene into styrene oxide. Under the optimum reaction condition, the yield of SO can reach 79.7% with a styrene conversion of 96.4% and a SO selectivity of 82.7%. The excellent catalytic performance of the CoFe_2O_4 nanoparticles over the monometallic Co_3O_4 flakes and Fe_2O_3 rods can be attributed to the synergistic effects between the adequate surface metal redox couples due to the bimetallic

nature and the mesoporous structure with large surface area. In addition with the attractive catalytic activity and product selectivity, the CoFe_2O_4 catalyst is magnetically separable and exhibits a good reusability. The findings in this work can be anticipated to open up new opportunities to the rational design of bimetallic or even multimetallic catalysts with earth-abundant elements for the styrene oxidation reaction and beyond.

Acknowledgements

This work was supported by the Natural Science Foundation of the Jiangsu Higher Education Institutions of China (17KJB530011), the Science and Technology Innovation Foundation of Yangzhou University (2017CXJ015), and the Priority Academic Program Development of Jiangsu Higher Education Institutions (PAPD).

Appendix A. Supplementary data

Supplementary material related to this article can be found, in the online version, at doi:<https://doi.org/10.1016/j.apcatb.2019.04.083>.

References

- [1] N. Agarwal, S.J. Freakley, R.U. McVicker, S.M. Althahban, N. Dimitratos, Q. He, D.J. Morgan, R.L. Jenkins, D.J. Willock, S.H. Taylor, C.J. Kiely, G.J. Hutchings, Aqueous Au-Pd colloids catalyze selective CH_4 oxidation to CH_3OH with O_2 under mild conditions, *Science* 358 (2017) 223–227.
- [2] P. Verma, K. Yuan, Y. Kuwahara, K. Mori, H. Yamashita, Enhancement of plasmonic activity by Pt/Ag bimetallic nanocatalyst supported on mesoporous silica in the hydrogen production from hydrogen storage material, *Appl. Catal., B* 223 (2018) 10–15.
- [3] M. Sankar, N. Dimitratos, P.J. Miedziak, P.P. Wells, C.J. Kiely, G.J. Hutchings, Designing bimetallic catalysts for a green and sustainable future, *Chem. Soc. Rev.* 41 (2012) 8099–8139.
- [4] X. Zhang, J. Ye, J. Yuan, T. Cai, B. Xiao, Z. Liu, K. Zhao, L. Yang, D. He, Excellent low-temperature catalytic performance of nanosheet Co-Mn oxides for total benzene oxidation, *Appl. Catal., A* 566 (2018) 104–112.
- [5] L. Zhao, Z. Zhang, Y. Li, X. Leng, T. Zhang, F. Yuan, X. Niu, Y. Zhu, Synthesis of Ce_aMnO_x hollow microsphere with hierarchical structure and its excellent catalytic performance for toluene combustion, *Appl. Catal., B* 245 (2019) 502–512.
- [6] H. Wang, C. Chen, H. Zhang, G. Wang, H. Zhao, An efficient and reusable bimetallic Ni_3Fe NPs@C catalyst for selective hydrogenation of biomass-derived levulinic acid to γ -valerolactone, *Chin. J. Catal.* 39 (2018) 1599–1607.
- [7] D. Yin, C. Han, X. Bo, J. Liu, L. Guo, Prussian blue analogues derived iron-cobalt alloy embedded in nitrogen-doped porous carbon nanofibers for efficient oxygen reduction reaction in both alkaline and acidic solutions, *J. Colloid Interface Sci.* 533 (2019) 578–587.
- [8] W. Zhong, M. Liu, J. Dai, J. Yang, L. Mao, D. Yin, Synergistic hollow CoMo oxide dual catalysis for tandem oxygen transfer: preferred aerobic epoxidation of cyclohexene to 1,2-epoxycyclohexane, *Appl. Catal., B* 225 (2018) 180–196.
- [9] A.H. Fakirah, A.S. Al-Fatesh, B. Chowdhury, A.A. Ibrahim, W.U. Khan, S. Hassan, K. Sasadeen, A.E. Abasaeed, Bi-metallic catalysts of mesoporous Al_2O_3 supported on Fe, Ni and Mn for methane decomposition: effect of activation temperature, *Chin. J. Chem. Eng.* 26 (2018) 1904–1911.
- [10] S.B. Kang, M. Hazlett, V. Balakotaiah, C. Kalamaras, W. Epling, Effect of Pt:Pd ratio on CO and hydrocarbon oxidation, *Appl. Catal., B* 223 (2018) 67–75.
- [11] Z. Yang, S. Pedireddy, H.K. Lee, Y. Liu, W.W. Tjiu, I.Y. Phang, X.Y. Ling, Manipulating the d-band electronic structure of platinum-functionalized

nanoporous gold bowls: synergistic intermetallic interactions enhance catalysis, *Chem. Mater.* 28 (2016) 5080–5086.

[12] J.R. Kitchin, J.K. Nørskov, M.A. Bartaeu, J.G. Chen, Role of strain and ligand effects in the modification of the electronic and chemical properties of bimetallic surfaces, *Phys. Rev. Lett.* 93 (2004) 156801.

[13] J.S. Kim, B. Kim, H. Kim, K. Kang, Recent progress on multimetal oxide catalysts for the oxygen evolution reaction, *Adv. Energy Mater.* 8 (2018) 1702774.

[14] G. Wang, Z. Wen, Self-supported bimetallic Ni–Co compound electrodes for urea- and neutralization energy-assisted electrolytic hydrogen production, *Nanoscale* 10 (2018) 21087–21095.

[15] X. Feng, J. Yang, X. Duan, Y. Cao, B. Chen, W. Chen, D. Lin, G. Qian, D. Chen, C. Yang, X. Zhou, Enhanced catalytic performance for propene epoxidation with H_2 and O_2 over bimetallic Au–Ag/Uncalcined titanium silicate-1 catalysts, *ACS Catal.* 8 (2018) 7799–7808.

[16] Z. Chen, B. Zhao, Y.-C. He, H.-R. Wen, X.-Z. Fu, R. Sun, C.-P. Wong, NiCo₂O₄ nanoframes with a nanosheet surface as efficient electrocatalysts for the oxygen evolution reaction, *Mater. Chem. Front.* 2 (2018) 1155–1164.

[17] W. Luo, L. Sun, Y. Yang, Y. Chen, Z. Zhou, J. Liu, F. Wang, Cu–Mn composite oxides: highly efficient and reusable acid–base catalysts for the carbonylation reaction of glycerol with urea, *Catal. Sci. Technol.* 8 (2018) 6468–6477.

[18] N. Masunga, G.S. Tito, R. Meijboom, Catalytic evaluation of mesoporous metal oxides for liquid phase oxidation of styrene, *Appl. Catal.*, A 552 (2018) 154–167.

[19] F. Pan, B. Zhang, W. Cai, The effect of hydrophilicity/hydrophobicity of TiO₂–SiO₂ composite aerogels in the epoxidation reaction, *Catal. Commun.* 98 (2017) 121–125.

[20] B. Li, X. Luo, J. Huang, X. Wang, Z. Liang, One-pot synthesis of ordered mesoporous Cu-KIT-6 and its improved catalytic behavior for the epoxidation of styrene: effects of the pH value of the initial gel, *Chin. J. Catal.* 38 (2017) 518–528.

[21] J. Sebastian, K.M. Jinka, R.V. Jasra, Effect of alkali and alkaline earth metal ions on the catalytic epoxidation of styrene with molecular oxygen using cobalt(II)-exchanged zeolite X, *J. Catal.* 244 (2006) 208–218.

[22] V. Chaudhary, Sweta, Synthesis and catalytic activity of SBA-15 supported catalysts for styrene oxidation, *Chin. J. Chem. Eng.* 26 (2018) 1300–1306.

[23] A.S. Sharma, H. Kaur, Alloying of AuNPs with palladium: A promising tool for tuning of selectivity for epoxide in oxidation of styrene using molecular oxygen, *Appl. Catal.*, A 546 (2017) 136–148.

[24] D.R. Godhani, H.D. Nakum, D.K. Parmar, J.P. Mehta, N.C. Desai, Zeolite Y engaged Ru(III) and Fe(III) complexes for oxidation of styrene, cyclohexene, limonene, and α -pinene: an eye-catching impact of H₂SO₄ on product selectivity, *J. Mol. Catal. A: Chem.* 426 (2017) 223–237.

[25] J. Liu, T. Chen, X. Yan, Z. Wang, R. Jian, P. Jian, E. Yuan, NiCo₂O₄ nanoneedle-assembled hierarchical microflowers for highly selective oxidation of styrene, *Catal. Commun.* 109 (2018) 71–75.

[26] H. Li, R. Hu, P. Yang, Y. He, J. Feng, D. Li, Synthesis of efficient Ce modified CuO/CoAl-HT catalysts for styrene epoxidation, *Catal. Lett.* 148 (2018) 1589–1596.

[27] J. Ren, X. Liu, R. Gao, W.-L. Dai, Morphology and crystal-plane effects of Zr-doped CeO₂ nanocrystals on the epoxidation of styrene with tert-butylhydroperoxide as the oxidant, *J. Energy Chem.* 26 (2017) 681–687.

[28] Q. Tang, Q. Zhang, H. Wu, Y. Wang, Epoxidation of styrene with molecular oxygen catalyzed by cobalt(II)-containing molecular sieves, *J. Catal.* 230 (2005) 384–397.

[29] Y. Li, S. Zhao, Q. Hu, Z. Gao, Y. Liu, J. Zhang, Y. Qin, Highly efficient Co₃S₄/SBA-15 catalysts prepared by atomic layer deposition for the epoxidation reaction of styrene, *Catal. Sci. Technol.* 7 (2017) 2032–2038.

[30] V.R. Choudhary, R. Jha, P. Jana, Selective epoxidation of styrene to styrene oxide by TBHP using simple transition metal oxides (NiO, CoO or MoO₃) as highly active environmentally-friendly catalyst, *Catal. Commun.* 10 (2008) 205–207.

[31] J. Liu, Z. Wang, P. Jian, R. Jian, Highly selective oxidation of styrene to benzaldehyde over a tailor-made cobalt oxide encapsulated zeolite catalyst, *J. Colloid Interface Sci.* 517 (2018) 144–154.

[32] F. Shi, M.K. Tse, M.-M. Pohl, A. Brückner, S. Zhang, M. Beller, Tuning catalytic activity between homogeneous and heterogeneous catalysis: improved activity and selectivity of free nano-Fe₂O₃ in selective oxidations, *Angew. Chem. Int. Ed.* 46 (2007) 8866–8868.

[33] F. Rajabi, N. Karimi, M.R. Saidi, A. Primo, R.S. Varma, R. Luque, Unprecedented selective oxidation of styrene derivatives using a supported iron oxide nanocatalyst in aqueous medium, *Adv. Synth. Catal.* 354 (2012) 1707–1711.

[34] A. de Brito, S. Neto, L.G. Pinheiro, J.M. Filho, A.C. Oliveira, Studies on styrene selective oxidation over iron-based catalysts: reaction parameters effects, *Fuel* 150 (2015) 305–317.

[35] R.A. Bepari, P. Bharali, B.K. Das, Controlled synthesis of α - and γ -Fe₂O₃ nanoparticles via thermolysis of PVA gels and studies on α -Fe₂O₃ catalyzed styrene epoxidation, *J. Saudi Chem. Soc.* 21 (2017) S170–S178.

[36] M.G. Clerici, O.A. Kholdeeva, *Liquid Phase Oxidation via Heterogeneous Catalysis: Organic Synthesis and Industrial Applications*, Wiley, 2013.

[37] S. Wang, Q. Li, M. Chen, W. Pu, Y. Wu, M. Yang, Electrochemical capacitance performance of Fe-doped Co₃O₄/graphene nanocomposite: investigation on the effect of iron, *Electrochim. Acta* 215 (2016) 473–482.

[38] R.S. Yadav, J. Havlica, M. Hnátko, P. Šajgalík, C. Alexander, M. Palou, E. Bartoníčková, M. Boháč, F. Frajkorová, J. Masilko, M. Zmrzlý, L. Kalina, M. Hajdúchová, V. Enev, Magnetic properties of Co_{1-x}Zn_xFe₂O₄ spinel ferrite nanoparticles synthesized by starch-assisted sol–gel auto-combustion method and its ball milling, *J. Magn. Magn. Mater.* 378 (2015) 190–199.

[39] P. Chandramohan, M.P. Srinivasan, S. Velmurugan, S.V. Narasimhan, Cation distribution and particle size effect on Raman spectrum of CoFe₂O₄, *J. Solid State Chem.* 184 (2011) 89–96.

[40] S. Singh, N. Khare, Defects/strain influenced magnetic properties and inverse of surface spin canting effect in single domain CoFe₂O₄ nanoparticles, *Appl. Surf. Sci.* 364 (2016) 783–788.

[41] J. Liu, S. Fang, R. Jian, F. Wu, P. Jian, Silylated Pd/Ti-MCM-41 catalyst for the selective production of propylene oxide from the oxidation of propylene with cumene hydroperoxide, *Powder Technol.* 329 (2018) 19–24.

[42] J. Liu, Z. Wang, X. Yan, P. Jian, Metallic cobalt nanoparticles imbedded into ordered mesoporous carbon: a non-precious metal catalyst with excellent hydrogenation performance, *J. Colloid Interface Sci.* 505 (2017) 789–795.

[43] K.-L. Yan, J.-F. Qin, J.-H. Lin, B. Dong, J.-Q. Chi, Z.-Z. Liu, F.-N. Dai, Y.-M. Chai, C.-G. Liu, Probing the active sites of Co₃O₄ for the acidic oxygen evolution reaction by modulating the Co²⁺/Co³⁺ ratio, *J. Mater. Chem. A* 6 (2018) 5678–5686.

[44] J. Liu, T. Chen, P. Jian, L. Wang, Hierarchical 0D/2D Co₃O₄ hybrids rich in oxygen vacancies as catalysts towards styrene epoxidation reaction, *Chin. J. Catal.* 39 (2018) 1942–1950.

[45] Z. Zhou, Y. Zhang, Z. Wang, W. Wei, W. Tang, J. Shi, R. Xiong, Electronic structure studies of the spinel CoFe₂O₄ by X-ray photoelectron spectroscopy, *Appl. Surf. Sci.* 254 (2008) 6972–6975.

[46] M. Li, Y. Xiong, X. Liu, X. Bo, Y. Zhang, C. Han, L. Guo, Facile synthesis of electrospun MFe₂O₄ (M = Co, Ni, Cu, Mn) spinel nanofibers with excellent electrocatalytic properties for oxygen evolution and hydrogen peroxide reduction, *Nanoscale* 7 (2015) 8920–8930.

[47] Q. Huang, P. Zhou, H. Yang, L. Zhu, H. Wu, In situ generation of inverse spinel CoFe₂O₄ nanoparticles onto nitrogen-doped activated carbon for an effective cathode electrocatalyst of microbial fuel cells, *Chem. Eng. J.* 325 (2017) 466–473.

[48] X. Zhao, Y. Fu, J. Wang, Y. Xu, J.-H. Tian, R. Yang, Ni-doped CoFe₂O₄ hollow nanospheres as efficient Bi-functional catalysts, *Electrochim. Acta* 201 (2016) 172–178.

[49] M.P. Gonzalez-Sandoval, A.M. Beesley, M. Miki-Yoshida, L. Fuentes-Cobas, J.A. Matutes-Aquino, Comparative study of the microstructural and magnetic properties of spinel ferrites obtained by co-precipitation, *J. Alloys Compd.* 369 (2004) 190–194.

[50] D. Ramimoghadam, S. Bagheri, A.T. Yousefi, S.B. Abd Hamid, Statistical optimization of effective parameters on saturation magnetization of nanomagnetite particles, *J. Magn. Magn. Mater.* 393 (2015) 30–35.

[51] S.K. Pardeshi, R.Y. Pawar, SrFe₂O₄ complex oxide an effective and environmentally benign catalyst for selective oxidation of styrene, *J. Mol. Catal. A: Chem.* 334 (2011) 35–43.

[52] W. Zhan, Y. Guo, Y. Wang, X. Liu, Y. Guo, Y. Wang, Z. Zhang, G. Lu, Synthesis of lanthanum-doped MCM-48 molecular sieves and its catalytic performance for the oxidation of styrene, *J. Phys. Chem. B* 111 (2007) 12103–12110.

[53] V.R. Choudhary, N.S. Patil, S.K. Bhargava, Epoxidation of styrene by anhydrous H₂O₂ over TS-1 and γ -Al₂O₃ catalysts: effect of reaction water, poisoning of acid sites and presence of base in the reaction mixture, *Catal. Lett.* 89 (2003) 55–62.

[54] S.C. Laha, R. Kumar, Selective epoxidation of styrene to styrene oxide over TS-1 using urea-hydrogen peroxide as oxidizing agent, *J. Catal.* 204 (2001) 64–70.

[55] X. Liu, J. Ding, X. Lin, R. Gao, Z. Li, W.-L. Dai, Zr-doped CeO₂ nanorods as versatile catalyst in the epoxidation of styrene with tert-butyl hydroperoxide as the oxidant, *Appl. Catal.*, A 503 (2015) 117–123.

[56] D.K. Dumbre, V.R. Choudhary, N.S. Patil, B.S. Upadhe, S.K. Bhargava, Calcium oxide supported gold nanoparticles as catalysts for the selective epoxidation of styrene by t-butyl hydroperoxide, *J. Colloid Interface Sci.* 415 (2014) 111–116.

[57] C. Huang, H. Zhang, Z. Sun, Y. Zhao, S. Chen, R. Tao, Z. Liu, Porous Fe₃O₄ nanoparticles: synthesis and application in catalyzing epoxidation of styrene, *J. Colloid Interface Sci.* 364 (2011) 298–303.

[58] Z. Pan, L. Hua, Y. Qiao, H. Yang, X. Zhao, B. Feng, W. Zhu, Z. Hou, Nanostructured maghemite-supported silver catalysts for styrene epoxidation, *Chin. J. Catal.* 32 (2011) 428–435.

[59] J. Liu, X. Yan, L. Wang, L. Kong, P. Jian, Three-dimensional nitrogen-doped graphene foam as metal-free catalyst for the hydrogenation reduction of *p*-nitrophenol, *J. Colloid Interface Sci.* 497 (2017) 102–107.

[60] C. Weerakkody, S. Biswas, W. Song, J. He, N. Wasalathantri, S. Dissanayake, D.A. Kriz, B. Dutta, S.L. Suib, Controllable synthesis of mesoporous cobalt oxide for peroxide free catalytic epoxidation of alkenes under aerobic conditions, *Appl. Catal.*, B 221 (2018) 681–690.

[61] L. Zhang, C. Liu, X. He, F. Zhang, Z. Zhang, Aerobic oxidation of styrene in functional reactors and computational fluid dynamics simulation, *Asia-Pac. J. Chem. Eng.* 13 (2018) e2206.

[62] J. Liu, T. Chen, P. Jian, L. Wang, X. Yan, Hollow urchin-like NiO/NiCo₂O₄ heterostructures as highly efficient catalysts for selective oxidation of styrene, *J. Colloid Interface Sci.* 526 (2018) 295–301.

[63] W. Li, Y. Hu, H. Jiang, N. Jiang, W. Bi, C. Li, Litchi-peel-like hierarchical hollow copper-ceria microspheres: aerosol-assisted synthesis and high activity and stability for catalytic CO oxidation, *Nanoscale* 10 (2018) 22775–22786.

[64] S. Lei, Q.-H. Li, Y. Kang, Z.-G. Gu, J. Zhang, Epitaxial growth of oriented prussian blue analogue derived well-aligned CoFe₂O₄ thin film for efficient oxygen evolution reaction, *Appl. Catal.*, B 245 (2019) 1–9.

[65] M. Konsolakis, M. Sgourakis, S.A.C. Carabineiro, Surface and redox properties of cobalt-ceria binary oxides: on the effect of Co content and pretreatment conditions, *Appl. Surf. Sci.* 341 (2015) 48–54.